Impact of local attenuation approximations when estimating correlation length from backscattered ultrasound echoes

Timothy A. Bigelow[a)]
Department of Electrical Engineering, University of North Dakota, Box 7165, Grand Forks, North Dakota 58202

William D. O'Brien, Jr.
Bioacoustics Research Laboratory, Department of Electrical and Computer Engineering, University of Illinois at Urbana—Champaign, 405 N. Mathews, Urbana, Illinois 61801

(Received 30 November 2005; revised 21 April 2006; accepted 7 May 2006)

Estimating the characteristic correlation length of tissue microstructure from the backscattered power spectrum could improve the diagnostic capability of medical ultrasound. Previously, size estimates were obtained after compensating for source focusing, the frequency-dependent attenuation along the propagation path (total attenuation), and the frequency-dependent attenuation in the scattering region (local attenuation). In this study, the impact of approximations of the local attenuation on the scatterer size estimate was determined using computer simulations and theoretical analysis. The simulations used Gaussian impedance distributions with an effective radius of 25 μm randomly positioned in a homogeneous half-space sonified by a spherically focused source ($f/1$ to $f/4$). The approximations of the local attenuation that were assessed neglected local attenuation (i.e., assume 0 dB/cm-MHz) neglected frequency dependence of the local attenuation, and assumed a finite frequency dependence (i.e., 0.5 dB/cm-MHz) independent of the true attenuation of the medium. Errors in the scatterer size estimate due to the local attenuation approximations increased with increasing window length, increasing true local attenuation and increasing f number. The most robust estimates were obtained when the local attenuation was approximated by a tissue-independent attenuation value that was greater than 70% of the largest attenuation expected in the tissue region of interest. [DOI: 10.1121/1.2208456]

PACS number(s): 43.80.Vj, 43.80.Ev, 43.80.Qf [FD] Pages: 546–553

LIST OF SYMBOLS

a_{eff} = effective radius, or correlation length, of scatterer
A_{comp} = generalized attenuation-compensation function including focusing effects along the beam axis
$a_{\text{eff}\,j}$ = estimated effective radius of scatterer found from one set (i.e., 25 averaged rf echoes) of simulated backscatter waveforms
$\bar{a}_{\text{eff}}$ = mean value of estimated effective radius from all sets of backscattered waveforms (i.e., $\bar{a}_{\text{eff}}=\Sigma_{\forall j} a_{\text{eff}\,j}/\Sigma_{\forall j} j$)
ASD = average squared difference term minimized when solving for a_{eff}
$E[\,]$ = expected value with respect to scattering random process
f = frequency
$F_\gamma(\omega, a_{\text{eff}})$ = form factor related to the scatterer geometry and effective radius
g_{win} = windowing function used to gate the time domain waveforms
k = wave number in tissue
L = equivalent length (in mm) of the windowing function used to gate the time domain waveforms
V_{plane} = backscattered voltage spectrum from rigid plane placed at the focal plane
w_z = equivalent Gaussian depth of focus of velocity potential field in focal region
V_{scat} = backscattered voltage spectrum from tissue containing scatterers
$X, \bar{X}$ = terms used in minimization scheme when solving for a_{eff}
z_T = distance from aperture plane to focal plane of ultrasound source
α_{high} = largest value of tissue attenuation expected
α_{loc} = frequency-dependent local attenuation in the scattering region of interest
α_{low} = smallest value of tissue attenuation expected
α_{ref} = frequency-dependent attenuation value selected for the local attenuation that is independent of the true value of α_{loc}
α_{tot} = frequency-dependent total attenuation along the propagation path for all tissue between focal plane and aperture plane
$\delta\alpha_{\text{loc}}$ = error between true α_{loc} value of the tissue and assumed α_{loc} value used in A_{comp} due to approximations in the value of α_{loc}

[a)]Electronic mail: timothybigelow@mail.und.nodak.edu

$\sigma_{a_{\text{lower}}}$ = percent deviation in values of scatterer effective radius for sizes smaller than the mean size (i.e., $a_{\text{eff}\,j} < \bar{a}_{\text{eff}}$)

$\sigma_{a_{\text{upper}}}$ = percent deviation in values of scatterer effective radius for sizes larger than the mean size (i.e., $a_{\text{eff}\,j} > \bar{a}_{\text{eff}}$)

ω = radian frequency

I. INTRODUCTION

Quantifying the underlying tissue structure using the information contained in the frequency spectrum of backscattered ultrasound echoes has been extensively studied (Chivers and Hill, 1975; Hall *et al.*, 1996; Insana *et al.*, 1990; Lizzi *et al.*, 1983; Nassiri and Hill, 1986; Oelze *et al.*, 2004). Typically, the spectra of the backscattered echoes are compared to a reference spectrum in order to estimate the characteristic correlation length (scatterer size) of the scatterers in the tissue while assuming a form factor that describes the correlation function. Once the correlation length has been determined, other parameters such as acoustic concentration (i.e., scatterer number density times their relative impedance change squared) can be estimated. Before the scatterer size can be determined, the backscattered spectra need to be compensated for frequency-dependent attenuation along the propagation path (total attenuation), frequency-dependent attenuation in the scattering region of interest (local attenuation), and focusing (Bigelow and O'Brien, 2004b).

Earlier publications (Bigelow and O'Brien, 2004a, b) demonstrated that the impact of attenuation and focusing can be compensated if the values of attenuation and effective Gaussian depth of focus are known. Although it may be possible to measure the effective Gaussian depth of focus for a source *a priori*, the attenuation varies drastically between patients even for the same tissue type. For example, many different attenuation coefficients for fat taken at different frequencies have been reported (Goss *et al.*, 1978). In particular, one study (Dussik and Fritch, 1956) gives attenuation values of 0.6 ± 0.2 dB/cm at 1 MHz and 2.3 ± 0.7 dB/cm at 5 MHz. Hence, for a change in frequency of 4 MHz, the change in attenuation varied from 0.8 to 2.6 dB/cm [i.e., $(2.3-0.7)$ dB/cm minus $(0.6+0.2)$ and $(2.3+0.7)$ dB/cm minus $(0.6-0.2)$ dB/cm], yielding attenuation slopes between 0.2 and 0.65 dB/cm-MHz. For this reason, an algorithm termed the Spectral Fit algorithm that estimated scatterer size and total attenuation simultaneously from the backscattered spectrum was developed (Bigelow *et al.*, 2005). The algorithm initially assumed weakly focused sources and utilized small window lengths to gate the time-domain echoes in order to reduce the importance of local attenuation and focusing. As a result, neither local attenuation nor focusing were included in the algorithm.

Before expanding the Spectral Fit algorithm to include focusing and local attenuation, the effect of different methods for correcting for these parameters when estimating the scatterer size needs to be determined. The impact of different corrections for focusing when the attenuation is known has already been quantified (Bigelow and O'Brien, 2004a, b). In this paper, the impact of different approximations of local attenuation on the scatterer size estimate is quantified using computer simulations and theoretical derivations. In the simulations, the total attenuation and effective Gaussian depth of focus are known, and three different approximations are used for the local attenuation value. First, local attenuation was completely neglected by assuming the local attenuation was zero when solving for the scatterer size. Second, the frequency dependence of the attenuation was neglected by assuming the local attenuation was the mean value of the attenuation over the frequency range of interest. Third, the local attenuation was assumed to have some finite frequency dependence (i.e., 0.5 dB/cm-MHz) independent of the true attenuation of the medium. The impact of each approximation of the local attenuation was then assessed by comparing the resulting scatterer size estimates for each against the size estimates that were obtained using the correct value of local attenuation for the same attenuation and degree of focusing.

Of the three estimates of attenuation considered in the analysis, the third case is of special interest because it is equivalent to the reference phantom technique that has also been implemented to correct for focusing (Gerig *et al.*, 2003). The reference phantom technique obtains time-gated signals about the focus from a phantom for use as a reference spectrum. All changes in the ultrasound field relevant to the focal region, including local attenuation, are included in the reference spectrum. Therefore, the technique is equivalent to assuming a specific frequency-dependent local attenuation equal to the attenuation of the phantom for all biological tissues independent of the true attenuation for the tissue. However, when using the reference phantom technique it is still critical to correct for total attenuation on a tissue-specific basis.

II. SIMULATION SETUP

A. Review of scatterer size estimation for focused sources

The scatterer radius, a_{eff}, is related to the backscattered power spectrum by (Bigelow and O'Brien, 2004b)

$$E[|V_{\text{scat}}|^2] \propto \frac{|k|^4 |V_{\text{plane}}(\omega)|^2}{A_{\text{comp}}(\omega)} F_\gamma(\omega, a_{\text{eff}}). \tag{1}$$

$V_{\text{plane}}(\omega)$ is the voltage spectrum that would be returned from a rigid plane placed at the focal plane in a water bath and is obtained independently to calibrate the echoes from the tissue. $F_\gamma(\omega, a_{\text{eff}})$ is the form factor describing the correlation function for the tissue, and the functional form of the form factor must be assumed before the scatterer size can be obtained. $A_{\text{comp}}(\omega)$ is a generalized attenuation-compensation function that corrects for focusing, local attenuation, and total attenuation and is given by (Bigelow and O'Brien, 2004b)

$$A_{\text{comp}} = \frac{e^{4\alpha_{\text{tot}} z_T}}{\int_{-L/2}^{L/2} ds_z (g_{\text{win}}(s_z) e^{4s_z^2/w_z^2} e^{\alpha_{\text{loc}} s_z})}. \quad (2)$$

Assuming that α_{tot}, α_{loc}, and w_z are known, the scatterer size can be determined by finding the value of a_{eff} that minimizes (Bigelow and O'Brien, 2004b),

$$\text{ASD} = \underset{\omega}{\text{mean}}[(X(\omega, a_{\text{eff}}) - \bar{X}(a_{\text{eff}}))^2], \quad (3)$$

where

$$X = \ln(E[|V_{\text{scat}}|^2]) - \ln(k^4 |V_{\text{plane}}|^2 F_\gamma(\omega, a_{\text{eff}})/A_{\text{comp}}),$$

$$\bar{X} = \underset{\omega}{\text{mean}}[X(f, a_{\text{eff}})]. \quad (4)$$

An estimate for $E[|V_{\text{scat}}|^2]$ is obtained by averaging the amplitude of the power spectra from adjacent echoes windowed in the time domain. The windowing restricts the depth resolution along the beam axis to the current tissue region of interest. Subtracting by $\bar{X}$ removes the effects of any multiplicative constants allowing for the estimation of scatterer size independent of the acoustic concentration.

B. Simulation parameters

The impact of different approximations for α_{loc} was tested by simulating the echoes generated by scatterers with Gaussian correlation functions [i.e., form factor of $F_\gamma(f, a_{\text{eff}}) = \exp(-0.827(ka_{\text{eff}})^2)$] randomly positioned in a homogeneous attenuating half-space. The attenuation of the half-space was varied from 0.05 to 1 dB/cm-MHz to test the impact of the approximations for different attenuation values. The scatterers were placed at a density of 35/mm^3 throughout the three-dimensional focal region with an a_{eff} of 25 μm. The sources used in the simulations had a focal length of 5 cm and f numbers of 1, 2, or 4, yielding 0.3, 1.2, and 4.8 scatterers per resolution cell, respectively. However, earlier simulations demonstrated that the scatterer size estimate was not strongly dependent on the number of scatterers per resolution cell (Bigelow and O'Brien, 2004b). The f number was varied to assess the impact of focusing in conjunction with the impact of α_{loc}. For all of the sources, the spectrum returned from a plane placed at the focal plane was

$$|V_{\text{plane}}(f)| \propto |f|^2 \exp\left(-2\left(\frac{f - 8\ \text{MHz}}{6\ \text{MHz}}\right)^2\right), \quad (5)$$

yielding ka_{eff} values corresponding to the maximum of the backscattered power spectrum ranging from ~1.3 to ~0.35 depending on the attenuation of the half-space. The optimal range for ka_{eff} values is between 1.2 and 0.5 (Insana and Hall, 1990).

For each f number and half-space attenuation value, 1000 different random distributions of scatterers were generated. The resultant echoes from each distribution were then grouped into sets of 25 waveforms for a total of 40 sets. Each waveform was then windowed in the time domain (providing resolution along the beam axis) and Fourier transformed to obtain the frequency spectrum. The spectra for all 25 waveforms in a set were then averaged to obtain $E[|V_{\text{scat}}|^2]$ for all 40 sets. Hence, 40 independent estimates of scatterer size were obtained for each simulated case. After averaging, $E[|V_{\text{scat}}|^2]$ needed to be compensated for spectral distortions (i.e., convolution with the windowing function in the frequency domain) introduced by the windowing. The convolution-related spectral distortions are different from the windowing effects compensated by A_{comp} in Eq. (2). The windowing compensation involves approximating $E[|V_{\text{scat}}|^2]$ and the Fourier transform of the windowing function as Gaussian functions. Then, the effect of windowing can be removed by multiplying the measured backscattered power spectrum by an appropriate Gaussian transformation (Bigelow and O'Brien, 2005b).

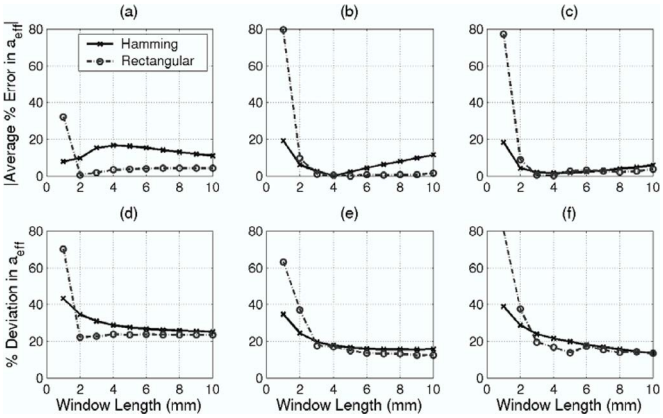

FIG. 1. Comparison of rectangular and Hamming windowing functions in terms of (a) accuracy and (d) precision of a_{eff} estimates for an $f/1$ transducer, (b) accuracy and (e) precision of a_{eff} estimates for an $f/2$ transducer, and (c) accuracy and (f) precision of a_{eff} estimates for an $f/4$ transducer for a half-space attenuation of 1 dB/cm-MHz without any approximations in the attenuation values.

C. Impact of different windowing functions

Prior to assessing the impact of the approximations for α_{loc}, the performance of two different windowing functions, the Hamming window and the rectangular window, were compared. A Hamming windowing function had been used when investigating the Spectral Fit algorithm (Bigelow and O'Brien, 2005b; Bigelow *et al.*, 2005) while a rectangular windowing function was used when developing the generalized attenuation-compensation function for use with focused sources (Bigelow and O'Brien, 2004a, b). The results for both types of windowing function are shown in Fig. 1 versus resolution along the beam axis. The half-space attenuation for these simulations was 1 dB/cm-MHz while α_{tot}, α_{loc}, and w_z were known exactly when applying A_{comp}. The average error was found by comparing the average value of all 40 estimates to the true value of a_{eff}. Likewise, the deviation was found by adding the standard deviations for estimates above and below the average value (i.e., $\sigma_{a_{\text{lower}}} + \sigma_{a_{\text{upper}}}$) as given by

$$\sigma_{a_{\text{upper}}} = \frac{100}{a_{\text{eff}}|_{\text{Theory}}} \sqrt{\frac{\sum_{\forall a_{\text{eff}j} > \bar{a}_{\text{eff}}} (a_{\text{eff}j} - \bar{a}_{\text{eff}})^2}{\sum_{\forall a_{\text{eff}j} > \bar{a}_{\text{eff}}} j}},$$

$$\sigma_{a_{\text{lower}}} = \frac{100}{a_{\text{eff}}|_{\text{Theory}}} \sqrt{\frac{\sum_{\forall a_{\text{eff}j} < \bar{a}_{\text{eff}}} (a_{\text{eff}j} - \bar{a}_{\text{eff}})^2}{\sum_{\forall a_{\text{eff}j} < \bar{a}_{\text{eff}}} j}}. \quad (6)$$

The calculation for the deviations was done using Eq. (6) because the deviations above the mean are typically different from the deviations below the mean (Bigelow and O'Brien, 2005a).

Except for small window lengths ($\leqslant$2 mm), the rectangular windowing function has better accuracy (smaller average % error) and better precision (smaller % deviation) than the Hamming windowing function, especially for the highly focused sources. The improvement with the rectangular windowing function may be related to the assumptions involved with the derivation of A_{comp} (Bigelow and O'Brien, 2004b) where it was assumed that the windowing function weighted the influence of the scatterers away from the focus along the beam axis. However, a complete analysis of the best windowing function is beyond the scope of this paper. Based on these results, a rectangular windowing function of length from 2 to 10 mm was selected for the remainder of the simulations.

III. RESULTS

A. Different approximations for α_{loc}

The impact of the different approximations for α_{loc} was investigated by solving for the scatterer size while using the approximate value for α_{loc} in the expression for A_{comp}. The size estimate from the approximate value for α_{loc} could then be compared to the size obtained for the correct value of α_{loc} for the same window length, half-space attenuation, and f number. Three different approximations for α_{loc} were considered. First, α_{loc} was neglected by setting it to 0 dB/cm-MHz in the calculation of A_{comp} regardless of the true value of α_{loc}. Second, the frequency dependence of α_{loc} was neglected by setting $\alpha_{\text{loc}} = \text{mean}_{\omega}(\alpha_{\text{loc}}(\omega))$ (i.e., constant α_{loc} without any frequency dependence). Third, α_{loc} was set to 0.5 dB/cm-MHz regardless of the true attenuation value.

The simulation results for all three variations in α_{loc} are shown with the results using the correct value of α_{loc} for window lengths of 3 and 6 mm in Figs. 2 and 3, respectively. Once again, the average error was found by comparing the average value of all 40 estimates to the true value of a_{eff}. Likewise, the deviation was found by adding the standard deviations for estimates above and below the average value (i.e., $\sigma_{a_{\text{lower}}} + \sigma_{a_{\text{upper}}}$) as given by Eq. (6). For the smaller window length of 3 mm (Fig. 2), the average errors in the size estimates [Figs. 2(a) and 2(c)] are all less than 5% except when the frequency dependence of α_{loc} was neglected [i.e., assumed $\alpha_{\text{loc}} = \text{mean}_{\omega}(\alpha_{\text{loc}}(\omega))$] for the $f/1$ transducer shown in Fig. 2(a). Similarly, the precision of the estimates for the different α_{loc} approximations [Figs. 2(d)–2(f)] is the same as the precision of the estimates when α_{loc} is known exactly

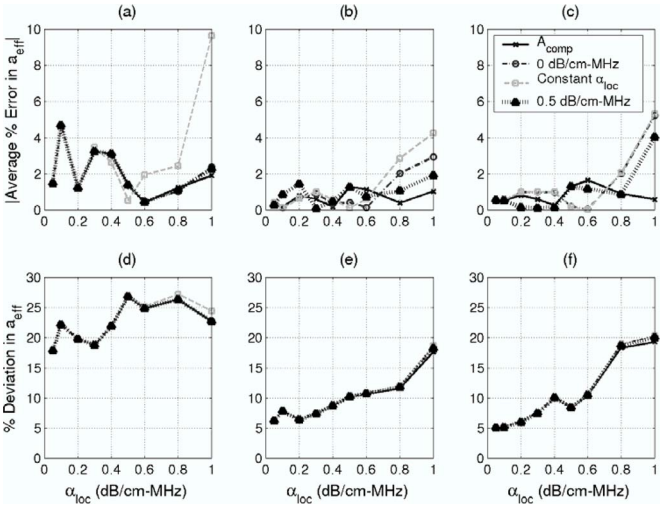

FIG. 2. Comparison between scatterer size estimates obtained when the local attenuation is known exactly (denoted A_{comp}), the local attenuation is neglected (denoted 0 dB/cm-MHz), the frequency dependence of the local attenuation is neglected (denoted constant α_{loc}), and the local attenuation is approximated by a tissue-independent value of 0.5 dB/cm-MHz in terms of (a) accuracy and (d) precision of a_{eff} estimates for an $f/1$ transducer, (b) accuracy and (e) precision of a_{eff} estimates for an $f/2$ transducer, and (c) accuracy and (f) precision of a_{eff} estimates for an $f/4$ transducer for a window length of 3 mm.

(denoted as A_{comp} in the figures). Hence, for small window lengths, the value used for α_{loc} does not affect the estimate of scatterer size.

For the larger window length of 6 mm (Fig. 3), there is a clear increase in the average errors in the size estimates as the true value of α_{loc} is increased for the $f/2$ and $f/4$ source. Hence, errors when approximating α_{loc} have a greater impact as the value of local attenuation increases. Except for when the frequency dependence of α_{loc} is neglected [i.e., assumed $\alpha_{\text{loc}} = \text{mean}_{\omega}(\alpha_{\text{loc}}(\omega))$], the average errors resulting from the

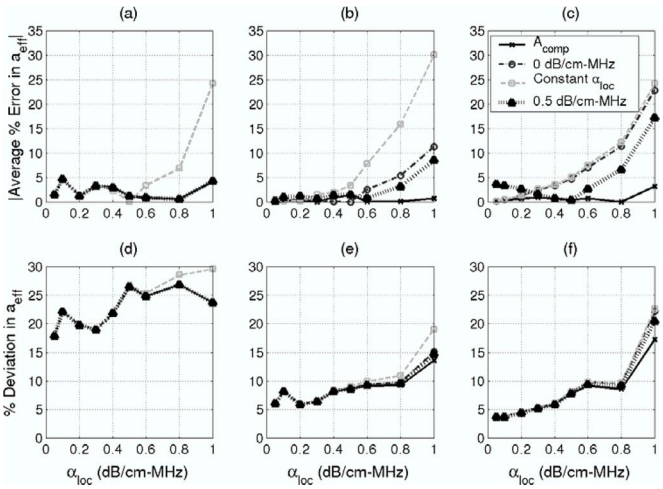

FIG. 3. Comparison between scatterer size estimates obtained when the local attenuation is known exactly (denoted A_{comp}), the local attenuation is neglected (denoted 0 dB/cm-MHz), the frequency dependence of the local attenuation is neglected (denoted constant α_{loc}), and the local attenuation is approximated by a tissue-independent value of 0.5 dB/cm-MHz in terms of (a) accuracy and (d) precision of a_{eff} estimates for an $f/1$ transducer, (b) accuracy and (e) precision of a_{eff} estimates for an $f/2$ transducer, and (c) accuracy and (f) precision of a_{eff} estimates for an $f/4$ transducer for a window length of 6 mm.

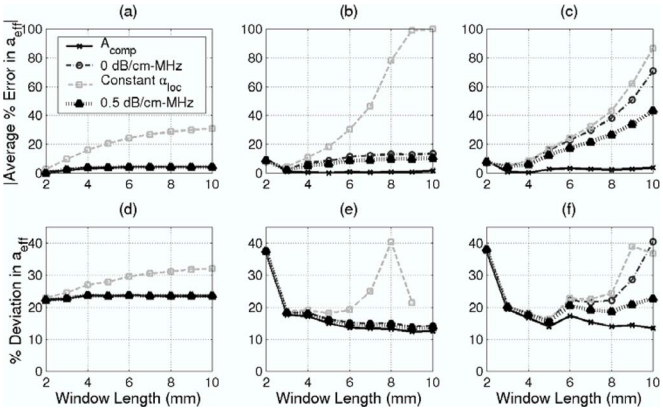

FIG. 4. Comparison between scatterer size estimates obtained when the local attenuation is known exactly (denoted A_{comp}), the local attenuation is neglected (denoted 0 dB/cm-MHz), the frequency dependence of the local attenuation is neglected (denoted constant α_{loc}), and the local attenuation is approximated by a tissue-independent value of 0.5 dB/cm-MHz in terms of (a) accuracy and (d) precision of a_{eff} estimates for an $f/1$ transducer, (b) accuracy and (e) precision of a_{eff} estimates for an $f/2$ transducer, and (c) accuracy and (f) precision of a_{eff} estimates for an $f/4$ transducer for a half-space attenuation of 1.0 dB/cm-MHz.

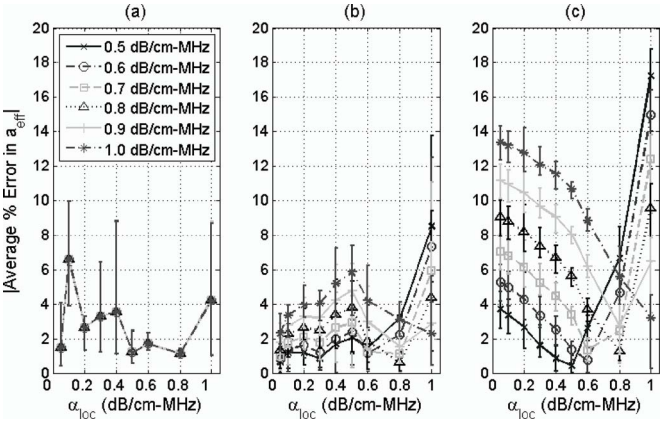

FIG. 5. Comparison of the accuracy of scatterer size estimates obtained when the local attenuation is approximated by a tissue-independent attenuation value of 0.5 to 1 dB/cm-MHz (denoted in legend) for an (a) $f/1$ transducer, (b) $f/2$ transducer, and (c) $f/4$ transducer for a window length of 6 mm.

approximations also decrease as the f number decreases (i.e., ~5% for $f/1$, ~10% for $f/2$, ~20% for $f/4$ for an α_{loc} of 1 dB/cm-MHz). Hence, the size estimates for the $f/1$ and $f/2$ sources exhibit a smaller dependence on the α_{loc} approximations. For the different approximations of α_{loc}, the errors are largest when the frequency dependence of α_{loc} is neglected (i.e., assumed $\alpha_{\text{loc}}=\text{mean}_{\omega}(\alpha_{\text{loc}}(\omega))$), and the next largest errors occur when α_{loc} is completely ignored (i.e., $\alpha_{\text{loc}}=0$ dB/cm-MHz). However, for the strongly focused sources, the errors when the frequency dependence of α_{loc} is neglected are much larger than the other errors while for the weakly focused sources all of the errors are comparable, indicating something different is happening for the weaker focused source. A tissue-independent attenuation value of 0.5 dB/cm-MHz gives the smallest errors for all of the true α_{loc} values and transducer f numbers.

The improved accuracy of the tissue-independent attenuation value and smaller f numbers can also be illustrated by the simulation results shown in Fig. 4 for a true α_{loc} value of 1 dB/cm-MHz for the different window lengths. Once again, the tissue-independent attenuation value of 0.5 dB/cm-MHz gives the smallest errors when compared to the estimates obtained with the other approximations [i.e., $\alpha_{\text{loc}}=\text{mean}_{\omega}(\alpha_{\text{loc}}(\omega))$ or $\alpha_{\text{loc}}=0$ dB/cm-MHz]. Also, the estimates obtained with the strongly focused sources are considerably better than the estimates obtained with the weaker focused source when α_{loc} is approximated except when the frequency dependence of α_{loc} is neglected, once again indicating that the source of error for weakly focused sources may be different than the source of error for the strongly focused sources. However, regardless of the desired resolution and true α_{loc} value, when approximating α_{loc}, using a strongly focused source and setting α_{loc} to 0.5 dB/cm-MHz in the attenuation-compensation calculation results in the most accurate estimates.

B. Variations in tissue-independent attenuation value

Although setting α_{loc} to 0.5 dB/cm-MHz was shown to give the most accurate estimates in the initial simulations when approximating the α_{loc} value, other values of tissue-independent attenuation might further improve the accuracy of the estimates. In this set of simulations, six different values for the tissue-independent attenuation were compared by finding the accuracy of the size estimates for true α_{loc} values from 0.05 to 1 dB/cm-MHz, window lengths from 2 to 10 mm, and f numbers of 1, 2, and 4. The values selected for the tissue-independent attenuation were 0.5, 0.6, 0.7, 0.8, 0.9, and 1 dB/cm-MHz. For these simulations, the variation in the accuracy was of interest so the 40 estimates were averaged in sets of ten estimates, each yielding four values for the average error of the size estimates.

The results for a window length of 6 mm for all of the different true α_{loc} values are shown in Fig. 5. The points correspond to the average percentage error of the four accuracy values while the error bars show the largest and smallest percentage errors of the four values. Once again, the most accurate estimates when α_{loc} is approximated are obtained for the smaller f-number transducers. However, the best value for the tissue-independent attenuation depends on the true α_{loc} value. Larger tissue-independent attenuation values give more accurate estimates when the true value of α_{loc} is large, while the smaller values for the tissue-independent attenuation give better estimates when the true value of α_{loc} is small. The smallest error in the estimates is obtained when the true value of α_{loc} is the same as the selected tissue-independent attenuation. Unfortunately, it is impossible to select an attenuation value that is always identical to the attenuation value of tissue due to biological variability.

To determine the best choice for the tissue-independent attenuation value when approximating α_{loc}, the maximum of the average errors over all values of α_{loc} (i.e., 0.05 to 1 dB/cm-MHz) is plotted versus window length in Fig. 6. The 40 estimates were still averaged in sets of ten to yield four values for the accuracy for each window length, tissue-independent attenuation value, and value of α_{loc}.

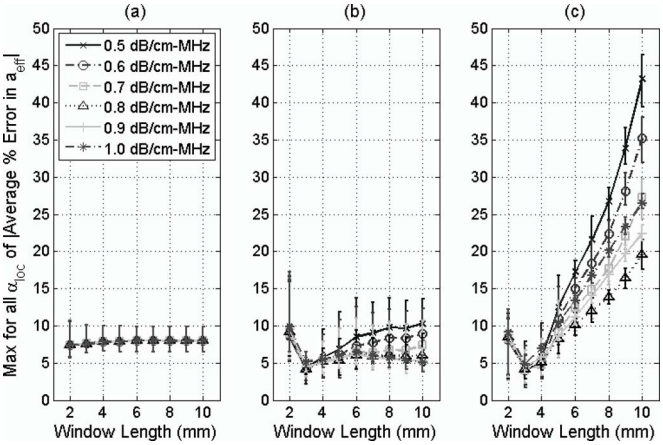

FIG. 6. Maximum average % error for the true α_{loc} values of 0.05 to 1 dB/cm-MHz when the local attenuation is approximated by a tissue-independent attenuation value of 0.5 to 1 dB/cm-MHz (denoted in legend) for an (a) $f/1$, (b) $f/2$, and (c) $f/4$ transducer.

Therefore, four values of the maximum of the average errors over all values of α_{loc} were obtained for each window length and tissue-independent attenuation value. The points in Fig. 6 correspond to the average of these four values while the error bars give the maximum and minimum.

For the $f/1$ and $f/2$ transducers [Figs. 6(a) and 6(b), respectively], all of the tissue-independent attenuation values give comparable error values with the possibility of subtle improvement for tissue-independent attenuation values of 0.7 to 1 dB/cm-MHz at larger window lengths. For the $f/4$ transducer [Fig. 6(c)], a tissue-independent attenuation value of 0.8 dB/cm-MHz gives consistently lower error values. Hence, 0.8 dB/cm-MHz would be the best choice for the tissue-independent attenuation when the biological variability is between 0.05 and 1 dB/cm-MHz. Notice that the best tissue-independent attenuation value is not in the middle of the range of the true α_{loc} values (i.e., not $\sim$0.5 dB/cm-MHz). This is probably due to the increased importance of errors in local attenuation at larger local attenuation values as was observed in Fig. 3.

C. Theoretical analysis of local attenuation approximations

The dependence of the error in the scatterer size estimate on approximations of the local attenuation value can also be analyzed by a theoretical analysis of the generalized attenuation-compensation function. For rectangular windowing functions, the influence of local attenuation on the estimate of the scatterer size is compensated by $\int_{-L/2}^{L/2} ds_z (e^{-4s_z^2/w_z^2} e^{4\alpha_{\mathrm{loc}} s_z})$. Because the performance of the strongly focused $f/1$ and $f/2$ sources in the simulations differed significantly from the performance for the $f/4$ source, an approximation for this integral was found for both highly focused and weakly focused sources.

First consider the limiting case when the length of the windowing function, L, is much greater than w_z as would be approximately true for the strongly focused $f/1$ and $f/2$ sources. The integral would then be given by

$$\int_{-L/2}^{L/2} ds_z \left(e^{\frac{4s_z^2}{w_z^2}} e^{4\alpha_{\mathrm{loc}} s_z} \right) \cong \frac{w_z\sqrt{\pi}}{2} e^{\alpha_{\mathrm{loc}}^2 w_z^2} = \frac{w_z\sqrt{\pi}}{2} e^{(\alpha_{\mathrm{loc}}^2|_{\mathrm{true}} + 2\delta\alpha\alpha_{\mathrm{loc}}|_{\mathrm{true}} + \delta\alpha^2) w_z^2}, \tag{7}$$

where $\delta\alpha$ is the error introduced by the approximation for α_{loc}. However, in order to impact scatterer size, $\delta\alpha$ must change the frequency dependence of the backscattered spectrum. Therefore, $(2\alpha_{\mathrm{loc}}|_{\mathrm{true}}\delta\alpha + \delta\alpha^2) w_z^2$ would need to have a dependence on frequency. Because w_z in the simulations and real tissue is approximately proportional to wavelength (Bigelow and O'Brien, 2004a, b), as long as $\delta\alpha$ and $\alpha_{\mathrm{loc}}|_{\mathrm{true}}$ are approximately proportional to frequency, the approximation would not impact the scatterer size estimate regardless of the difference between the assumed and true local attenuation value. This explains why the $f/1$ and $f/2$ sources yielded small errors in the scatterer size regardless of the approximation except when the approximation neglected the frequency dependence of the attenuation.

Now consider the limiting case when the windowing function, L, is much smaller than w_z as would be a rough approximation for the $f/4$ source. Under this limit, the integral would be given by

$$\int_{-L/2}^{L/2} ds_z (e^{-4s_z^2/w_z^2} e^{4\alpha_{\mathrm{loc}} s_z}) \cong \int_{-L/2}^{L/2} ds_z (e^{4\alpha_{\mathrm{loc}} s_z}) = \frac{e^{4\alpha_{\mathrm{loc}} L/2} - e^{-4\alpha_{\mathrm{loc}} L/2}}{4\alpha_{\mathrm{loc}}} = \frac{1}{2\alpha_{\mathrm{loc}}} \sinh(2\alpha_{\mathrm{loc}} L). \tag{8}$$

Because $2\alpha_{\mathrm{loc}} L \ll 1$, Eq. (8) can be further simplified to yield

$$\frac{1}{2\alpha_{\mathrm{loc}}} \sinh(2\alpha_{\mathrm{loc}} L) \cong L\left(1 + \frac{(2\alpha_{\mathrm{loc}} L)^2}{6}\right). \tag{9}$$

Therefore, the error in the scatterer size estimate due to the approximation for α_{loc} would be on the order of $L^2 2/3 |2\alpha_{\mathrm{loc}}|_{\mathrm{true}}\delta\alpha + \delta\alpha^2|$, which equals $L^2 2/3 |\alpha_{\mathrm{ref}} - \alpha_{\mathrm{loc}}|_{\mathrm{true}}| (\alpha_{\mathrm{ref}} + \alpha_{\mathrm{loc}}|_{\mathrm{true}})$ when written in terms of the tissue-independent attenuation value α_{ref}. Notice that this term increases as the true value of local attenuation and window length increase for the same $\delta\alpha$ as was also observed for the error in the size estimates in the computer simulations. The error term $C_{\mathrm{mse}} |\alpha_{\mathrm{ref}} - \alpha_{\mathrm{loc}}|_{\mathrm{true}}| (\alpha_{\mathrm{ref}} + \alpha_{\mathrm{loc}}|_{\mathrm{true}})$ for a α_{ref} of 0.7 dB/cm-MHz is also plotted with the corresponding curve from Fig. 5(c) in Fig. 7. C_{mse} is a scaling constant used to plot the curves on the same scale and was found by minimizing the mean squared error between the two curves. There is reasonable agreement between the theoretical error term and the simulated error curve except at higher attenuation values where the simulation error is larger than expected from the theory.

Assuming that the error due to the approximations for α_{loc} is approximately described by $L^2 2/3 |\alpha_{\mathrm{ref}} - \alpha_{\mathrm{loc}}|_{\mathrm{true}}|$

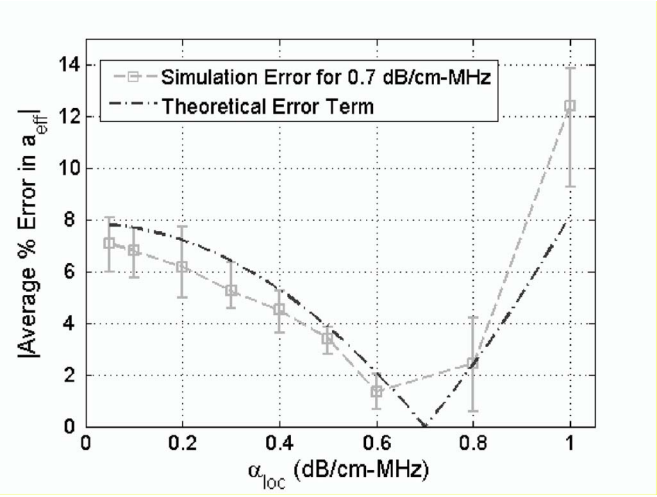

FIG. 7. Comparison between theoretical error term, $C_{mse}(|\alpha_{ref}-\alpha_{loc}|_{true}|(\alpha_{ref}+\alpha_{loc}|_{true}))$, and the accuracy of scatterer size estimates obtained when the local attenuation is approximated by a tissue-independent attenuation value of 0.7 dB/cm-MHz for an $f/4$ transducer for a window length of 6 mm.

$(\alpha_{ref}+\alpha_{loc}|_{true})$, it is possible to calculate the best value for α_{ref} given a range of expected $\alpha_{loc}|_{true}$ values. A plot of the $\max_{\forall \alpha_{loc}|_{true}}(|\alpha_{ref}-\alpha_{loc}|_{true}|(\alpha_{ref}+\alpha_{loc}|_{true}))$ vs. α_{ref} is shown in Fig. 8 for $\alpha_{loc}|_{true}$ values between 0.05 and 1 dB/cm -MHz. The plot consists of the intersection of two curves with the minimum value of $\max_{\forall \alpha_{loc}|_{true}}(|\alpha_{ref}-\alpha_{loc}|_{true}|(\alpha_{ref}+\alpha_{loc}|_{true}))$ occurring at the intersection. The curve with the negative slope corresponds to when the maximum error is due to large $\alpha_{loc}|_{true}$ values [i.e., $\max_{\forall \alpha_{loc}|_{true}}(|\alpha_{ref}-\alpha_{loc}|_{true}|(\alpha_{ref}+\alpha_{loc}|_{true}))=(\alpha_{high}^2-\alpha_{ref}^2)$ where $\alpha_{high}>\alpha_{ref}$], while the curve with the positive slope corresponds to when the maximum error is due to a small $\alpha_{loc}|_{true}$ values [i.e., $\max_{\forall \alpha_{loc}|_{true}}(|\alpha_{ref}-\alpha_{loc}|_{true}|(\alpha_{ref}+\alpha_{loc}|_{true}))=(\alpha_{ref}^2-\alpha_{low}^2)$ where $\alpha_{low}<\alpha_{ref}$]. α_{high} and α_{low} correspond to the largest and smallest values of local attenuation possible for a tissue region of interest, respectively. Because the minimum theoretical error value corresponds to the intersection, the minimum error should occur when

$$(\alpha_{high}^2-\alpha_{ref}^2)=(\alpha_{ref}^2-\alpha_{low}^2)\Rightarrow\alpha_{ref}=\sqrt{\frac{\alpha_{high}^2+\alpha_{low}^2}{2}}. \tag{10}$$

For the simulations presented in this paper, Eq. (10) would yield an optimal tissue-independent attenuation value of 0.71 dB/cm-MHz, which is slightly smaller than the optimal value of 0.8 dB/cm-MHz that was observed in Fig. 6. The small difference can be attributed to the theoretical error term being smaller than the real error value for the higher attenuation values as was observed in Fig. 7. Because the error due to the higher attenuation values will decrease as the tissue-independent attenuation value increases, it is reasonable to expect that the optimal tissue-independent attenuation value should be slightly larger than the value given by Eq. (10).

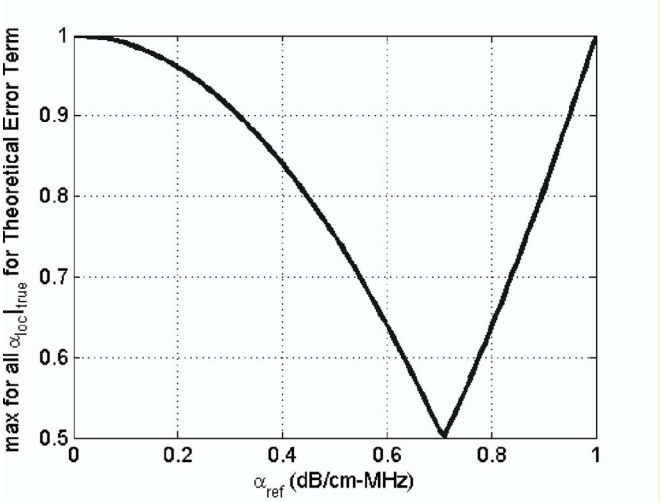

FIG. 8. Value of $\max_{\forall \alpha_{loc}|_{true}}(|\alpha_{ref}-\alpha_{loc}|_{true}|(\alpha_{ref}+\alpha_{loc}|_{true}))$ for α_{loc} values of 0.05 to 1 dB/cm-MHz when the local attenuation is approximated by a tissue-independent attenuation value, α_{ref}.

IV. CONCLUSIONS

Although it is well known that correcting for the frequency-dependent attenuation both along the propagation path (total attenuation) and in the scattering region (local attenuation) is critical when estimating the correlation length of tissue microstructure, the impact of approximations of the local attenuation on the estimate has not been addressed. In this investigation, three different types of approximations for the local attenuation were assessed using computer simulations and theoretical analysis. First, the local attenuation was completely neglected (i.e., $\alpha_{loc}=0$ dB/cm-MHz regardless of the true attenuation value). Second, the frequency dependence of the local attenuation was neglected [i.e., $\alpha_{loc}=\text{mean}_{\omega}(\alpha_{loc}(\omega))$]. Third, the local attenuation was approximated by a tissue-independent attenuation value (i.e., $\alpha_{loc}=0.5$ dB/cm-MHz regardless of the true attenuation value). Errors in the scatterer size estimate due to the approximations were shown to increase with increasing window length, increasing true local attenuation, and increasing f number provided that the frequency dependence of the attenuation was not ignored. The most robust estimates were obtained when the local attenuation was approximated by a tissue-independent attenuation value.

After demonstrating that the tissue-independent attenuation yielded the best results when the local attenuation was being approximated, the optimal choice for the tissue-independent attenuation was determined using computer simulations and theoretical calculations. In the computer simulations, six different reference attenuation values (0.5, 0.6, 0.7, 0.8, 0.9, and 1 dB/cm-MHz) were compared for true attenuation values ranging from 0.5 to 1 dB/cm-MHz. The largest error over all of the true local attenuation values for each value of the tissue-independent attenuation was then used to quantify the performance of each tissue-independent attenuation value. The calculations and simulations showed that the optimal value for the tissue-independent attenuation was slightly larger than $\sqrt{(\alpha_{high}^2+\alpha_{low}^2)/2}$ where α_{high} and α_{low} correspond to the largest and smallest values of local

attenuation expected for a tissue region of interest, respectively. The optimal tissue-independent attenuation value being slightly larger than $\sqrt{(\alpha_{\text{high}}^2+\alpha_{\text{low}}^2)/2}$ results from the current theory not adequately capturing the error performance at higher attenuation values. However, $\sqrt{(\alpha_{\text{high}}^2+\alpha_{\text{low}}^2)/2}$ still serves as a good choice for the tissue-independent attenuation value, especially when operating at smaller window lengths and/or using strongly focused sources.

ACKNOWLEDGMENTS

This work was supported by the University of Illinois Research Board and the University of North Dakota School of Engineering and Mines.

Bigelow, T. A., and O'Brien, W. D., Jr. (**2004a**). "Scatterer size estimation in pulse-echo ultrasound using focused sources: Calibration measurements and phantom experiments," J. Acoust. Soc. Am. **116**, 594–602.

Bigelow, T. A., and O'Brien, W. D., Jr. (**2004b**). "Scatterer size estimation in pulse-echo ultrasound using focused sources: Theoretical approximations and simulation analysis," J. Acoust. Soc. Am. **116**, 578–593.

Bigelow, T. A., and O'Brien, W. D., Jr. (**2005a**). "Evaluation of the spectral fit algorithm as functions of frequency range and Δka_{eff}," IEEE Trans. Ultrason. Ferroelectr. Freq. Control **52**, 2003–2010.

Bigelow, T. A., and O'Brien, W. D., Jr. (**2005b**). "Signal processing strategies that improve performance and understanding of the quantitative ultrasound SPECTRAL FIT algorithm," J. Acoust. Soc. Am. **118**, 1808–1819.

Bigelow, T. A., Oelze, M. L., and O'Brien, W. D., Jr. (**2005**). "Estimation of total attenuation and scatterer size from backscattered ultrasound waveforms," J. Acoust. Soc. Am. **117**, 1431–1439.

Chivers, R. C., and Hill, C. R. (**1975**). "A spectral approach to ultrasonic scattering from human tissue: methods, objectives and backscattering measurements," Phys. Med. Biol. **20**, 799.

Dussik, K. T., and Fritch, D. J. (1956). "Determination of sound attenuation and sound velocity in the structure constituting the joints, and of the ultrasonic field distribution within the joints on living tissues and anatomical preparations, both in normal and pathological conditions," Public Health Service, Natl. Inst. Health Project A454, Prog. Rep. (15 September, 1956).

Gerig, A., Zagzebski, J., and Varghese, T. (**2003**). "Statistics of ultrasonic scatterer size estimation with a reference phantom," J. Acoust. Soc. Am. **113**, 3430–3437.

Goss, S. A., Johnston, R. L., and Dunn, F. (**1978**). "Comprehensive compilation of empirical ultrasonic properties of mammalian tissues," J. Acoust. Soc. Am. **64**, 423–457.

Hall, T. J., Insana, M. F., Harrison, L. A., and Cox, G. G. (**1996**). "Ultrasonic measurement of glomerular diameters in normal adult humans," Ultrasound Med. Biol. **22**, 987–997.

Insana, M. F., and Hall, T. J. (**1990**). "Parametric ultrasound imaging from backscatter coefficient measurements: Image formation and interpretation," Ultrason. Imaging **12**, 245–267.

Insana, M. F., Wagner, R. F., Brown, D. G., and Hall, T. J. (**1990**). "Describing small-scale structure in random media using pulse-echo ultrasound," J. Acoust. Soc. Am. **87**, 179–192.

Lizzi, F. L., Greenebaum, M., Feleppa, E. J., Elbaum, M., and Coleman, D. J. (**1983**). "Theoretical framework for spectrum analysis in ultrasonic tissue characterization," J. Acoust. Soc. Am. **73**, 1366–1373.

Nassiri, D. K., and Hill, C. R. (**1986**). "The use of angular acoustic scattering measurements to estimate structural parameters of human and animal tissues," J. Acoust. Soc. Am. **79**, 2048–2054.

Oelze, M. L., O'Brien, W. D., Jr., Blue, J. P., and Zachary, J. F. (**2004**). "Differentiation and characterization of rat mammary fibroadenomas and 4T1 mouse carcinomas using quantitative ultrasound imaging," IEEE Trans. Med. Imaging **23**, 764–771.